

Miniature Compliant Grippers with Force-Sensing

N. Maheshwari¹, A. Narayana Reddy^{2*}, Deepak Kumar Sahu^{2,3} and G.K. Ananthasuresh²

Multi-disciplinary and Multi-scale Device and Design (M2D2) Laboratory

¹Department of Mechanical Engineering, Indian Institute of Technology Madras, Chennai, India

²Department of Mechanical Engineering, Indian Institute of Science, Bangalore, India

³(Current address) John F. Welch Technology Centre, General Electric, Bangalore, India

* Corresponding author (email: anreddy@mecheng.iisc.ernet.in)

Abstract

This paper is concerned with the manipulation of biological cells with miniature grippers that can also measure forces. We have designed three single-piece, compliant miniature grippers with parallel and angular jaw motions. Two grippers were designed intuitively while the third one was designed using topology optimization with implicit manufacturing constraints. These grippers were fabricated using different manufacturing techniques as well as with different materials. We present a vision-based force-sensing method by solving Cauchy's problem in elasticity. In this work, the gripper was used to hold a yeast ball of less than 1 mm in diameter and forces involved there in were estimated to be about 30 mN. The force-sensing technique was validated at the macro scale where there was an independent method of estimating the forces using spring arrangement.

Keywords: Micro-gripper, micromanipulation, topology optimization, prototyping, Cauchy's problem, vision-based force-sensing.

1 Introduction

Manipulating individual biological cells is useful in sperm injection, intracellular DNA injection, and in mechanical characterization. There are several non-contact biomanipulation techniques such as laser trapping, electro-rotation, etc., [1-3] to handle micron-sized objects. However, these techniques cause damage to the cell and thereby lead to undesirable effects. Conventionally, manipulation of biological cells is done using micropipettes through aspiration [4]. The autonomous embryo injection system has been developed to eliminate direct human involvement in this process [5]. The use of a micro-gripper equipped with a piezoelectric actuator was demonstrated for biomanipulation and handling of embryos [6,7]. In this paper, we focus on using micro-grippers that are designed to match the stiffness of the objects handled as well as with force-sensing capability.

The design of microgrippers can be done intuitively or by using topology optimization. In this work, we present three designs of grippers based on intuition as well as topology optimization. The intuitively conceived

grippers have parallel jaw motion whereas the topology optimized gripper has angular motion. The manufacturing constraints were incorporated implicitly in the design of a gripper obtained using topology optimization [8].

We have also incorporated vision-based force-sensing for manipulation of biological objects using miniature compliant grippers. It is a non-intrusive technique for sensing force, as we do not mount any force sensors [9-12]. Instead, we take advantage of the elastic deformation of the compliant gripper itself to compute the forces. Displacements of the gripper are extracted at selected locations by comparing images before and after the deformation, which are captured either by a camera or a camera attached to a microscope. After extracting the displacements, we solve Cauchy's problem in elasticity to get the forces acting on the gripper as well as the grasped object. To solve this problem, we have to minimize spurious forces that appear at selected measurement locations using constrained optimization [12]. In this paper, we discuss the Newton's method as an alternative to constrained optimization to minimize the spurious forces. The advantage of the Newton's method is that we need not specify the accuracy of displacement-measurement technique.

The grippers were prototyped using spring steel and polydimethylsiloxane (PDMS). These grippers were fabricated in three different ways: wire-cut Electric Discharge Machining (EDM) and photolithography for spring steel; and vacuum casting for PDMS. The fabricated grippers were tested on various biological objects such as zebrafish egg-cells, drosophila embryos, yeast balls, and hibiscus pollen. We were able to not only grasp but also roll, squeeze, and stretch the aforementioned biological objects. The validation of force-sensing techniques is also presented in this paper.

The remainder of the paper is organized as follows. In Section 2, we present the design and analysis of grippers based on intuition and topology optimization. In Section 3, the concept of force-sensing technique used for calculating the forces is discussed. In Section 4, we present the details of the fabricated grippers. Section 5 contains a description of the experiments carried out on biological objects using spring steel and PDMS grippers. Section 6 presents the computation and validation of the force-sensing experiments. The paper concludes with Section 7.

2 Design and analysis of grippers

2.1 Intuitive gripper design

The constraint for this design was that gripper jaws should move parallel to each other with equal displacements throughout the range of motion. The parallel jaw motion is preferred over angular motion as the gripping action does not produce a force in a direction to eject the cell from the jaws. The initial design was conceived intuitively and a beam finite element model was used to check the deformation of the structure using in-house finite element code developed in MATLAB. After the concept was finalized, the gripper was modeled in solid modeling software, SolidWorks, and the effect of different design variables such as the beam width, the angle between beams, the number of beams, etc., were studied. The stress concentration and deformation patterns were analyzed in a continuum version of the design created in COMSOL MultiPhysics, commercially available finite element software. For analysis purposes, one of the gripper jaws was considered fixed to calculate the overall jaw displacement. After several iterations, an optimal gripper design was selected on the basis of mechanical efficiency, stiffness of the mechanism, and stress concentration. For equal displacement of jaws, the gripper needs to be symmetrically actuated at two points. The design for two spring steel grippers with different stiffness characteristics is shown in Figs.1a-b. The grippers had, respectively, a stiffness of 3,367 N/m and 10,917 N/m. This shows that the stiffness can be considerably altered to suit the requirement.

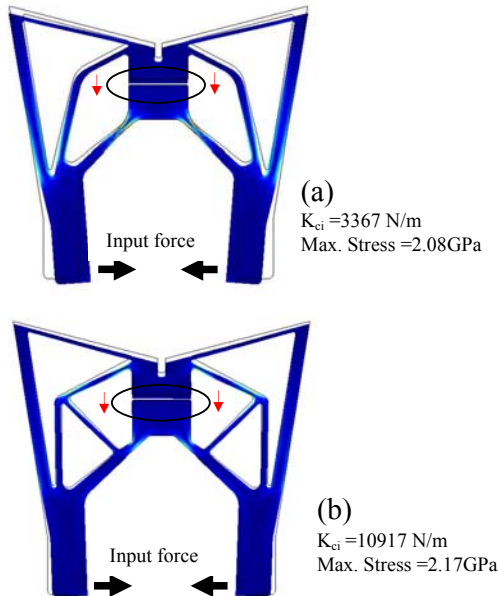


Fig. 1: Stress plot for parallel jaw motion grippers.

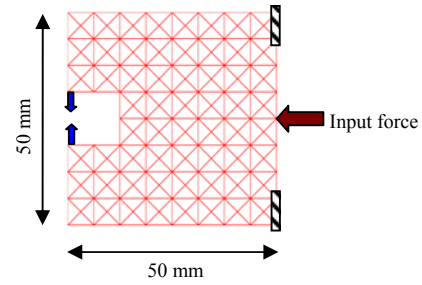


Fig. 2: The ground structure of frame finite elements used for topology optimization.

2.2 Topologically optimized gripper design

Topology optimization is a systematic method to obtain a compliant mechanism for a specific objective. The objective of the mechanism in this case is a gripper. We have used frame finite elements to model the mechanism and the ground structure of the design as shown in Fig. 2. The constraint posed by minimum feature of manufacturing technique was implicitly taken into account in the design process.

The statement of the topology optimized problem is as follows:

$$\text{Maximize}_w \frac{MSE}{SE} = \frac{\mathbf{V}^T \mathbf{K} \mathbf{U}}{0.5 \mathbf{U}^T \mathbf{K} \mathbf{U}}$$

Subject to

$$\sum_{i=1}^{NELEM} t w_i l_i - V^* \leq 0$$

$$\mathbf{K} \mathbf{U} = \mathbf{F}$$

$$\mathbf{K} \mathbf{V} = \mathbf{F}_d$$

where MSE is the mutual strain energy that is numerically equal to the output displacement, SE is the strain energy that is a measure of stiffness, \mathbf{K} is the stiffness matrix of the finite element model, \mathbf{U} and \mathbf{V} are displacements for the actual load \mathbf{F} applied at the input degree of freedom and unit dummy load \mathbf{F}_d applied at the output degree of freedom respectively, A_i contains the areas of cross-section of the frame elements, l_i contains the length of the frame elements, t is thickness of the structure, and finally V^* is the allowed volume of material to be used by the mechanism. The design variables are smooth approximation of the Heaviside function convoluted with a ramp function, which takes care of the manufacturing considerations on minimum width [8]. The new design parameterization function is shown in Eq. (1) and the plot of the function is shown in Fig. 3.

$$W(\rho) = \frac{\rho}{1 + e^{-a(\rho - c)}} \quad (1)$$

Where ρ is a design variable and W is width of a frame element.

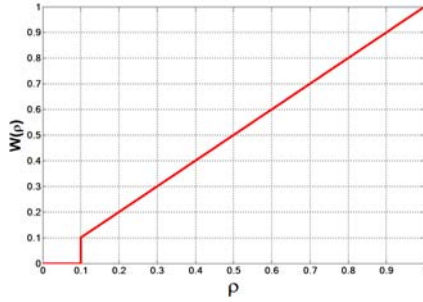


Fig. 3: A plot of the width of a frame element vs. the design variable. There is no non-smoothness at the corner because the Heaviside function is smoothly approximated.

A design obtained using optimization is analyzed with continuum elements using COMSOL MultiPhysics software and is shown in Fig. 4. Further details are in [8].

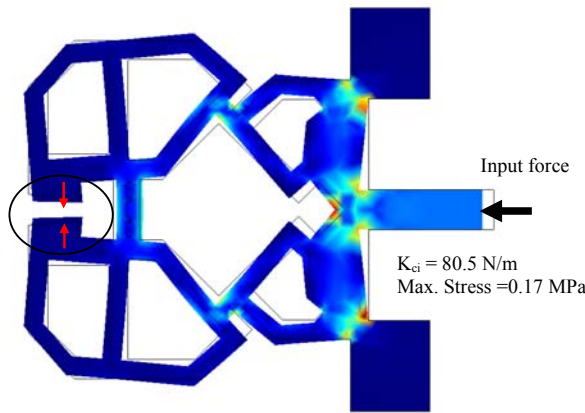


Fig. 4: The von Mises stress plot in the deformed configuration of the topology-optimized gripper.

3 The Force-sensing Method

As discussed in the introduction, we use vision-based force-sensing for estimating the forces of manipulation. The formulation of Cauchy's problem is presented in this section. The gripper being an elastic body, it can be schematically represented as shown in Fig. 5.

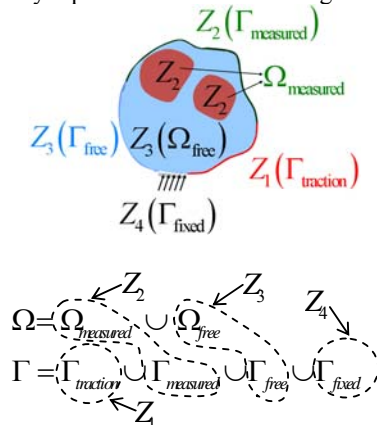


Fig. 5: Schematically shown elastic body with partitions of domain and boundary.

Domain Ω and boundary Γ of the elastic body are partitioned into four regions: the first region is the one where forces act (Γ_{traction}); the second region is where displacements are measured ($\Omega_{\text{measured}} \cup \Gamma_{\text{measured}}$); the third region is where we do not know the displacements but know the forces ($\Omega_{\text{free}} \cup \Gamma_{\text{free}}$); and the fourth region is where the displacements are fixed. All these partitions are shown in Fig. 5.

The mathematical statement of the Cauchy's problem is as follows.

$$\nabla \cdot \tilde{\mathbf{T}} = 0 \quad \text{in } \Omega \quad (2a)$$

$$\tilde{\mathbf{T}} = \lambda \text{tr}(\tilde{\mathbf{E}})\tilde{\mathbf{I}} + 2\mu\tilde{\mathbf{E}} \quad (2b)$$

$$\tilde{\mathbf{E}} = \frac{1}{2}(\nabla\mathbf{U} + \nabla\mathbf{U}^T + \nabla\mathbf{U}^T\nabla\mathbf{U}) \quad (2c)$$

$$\mathbf{U} = 0 \quad \text{on } \Gamma_{\text{fixed}} \quad (2d)$$

$$\mathbf{t} = 0 \quad \text{on } \Gamma_{\text{measured}} \cup \Gamma_{\text{free}} \quad (2e)$$

$$\mathbf{U} = \mathbf{U}_{\text{measured}} \quad \text{on } \Omega_{\text{measured}} \cup \Gamma_{\text{measured}} \quad (2f)$$

where $\tilde{\mathbf{T}}$ is the second Piola-Kirchhoff stress tensor, $\tilde{\mathbf{I}}$ the identity tensor, $\tilde{\mathbf{E}}$ the Green strain tensor, λ and μ the Lame constants of the material, \mathbf{U} the displacement vector, \mathbf{t} the traction, and $\mathbf{U}_{\text{measured}}$ the measured displacement vector.

Static equilibrium is achieved when internal forces \mathbf{F}_{int} balance the external forces \mathbf{F}_{ext} . That is,

$$\mathbf{F}_{\text{int}} = \mathbf{F}_{\text{ext}} \quad (3)$$

The internal force vector (\mathbf{F}_{int}) is a nonlinear function of the displacements because we consider geometric nonlinearity in the problem. By using the first order Taylor series for \mathbf{F}_{int} , we get:

$$\mathbf{F}_{\text{int}} + \frac{\partial \mathbf{F}_{\text{int}}}{\partial \mathbf{u}} \Delta \mathbf{u} = \mathbf{F}_{\text{int}} + \mathbf{K}_T \Delta \mathbf{u} = \mathbf{F}_{\text{ext}} \quad (4)$$

where \mathbf{K}_T is the tangent stiffness matrix, which depends on \mathbf{u} in geometrically nonlinear problems.

$$\mathbf{K}_T \Delta \mathbf{u} = \mathbf{F}_{\text{ext}} - \mathbf{F}_{\text{int}} \Rightarrow \begin{bmatrix} \mathbf{K}_{11} & \mathbf{K}_{12} & \mathbf{K}_{13} \\ \mathbf{K}_{21} & \mathbf{K}_{22} & \mathbf{K}_{23} \\ \mathbf{K}_{31} & \mathbf{K}_{32} & \mathbf{K}_{33} \end{bmatrix} \begin{Bmatrix} \Delta \mathbf{u}_1 \\ \Delta \mathbf{u}_2 \\ \Delta \mathbf{u}_3 \end{Bmatrix} = \begin{Bmatrix} \mathbf{F}_1 \\ \mathbf{0} \\ \mathbf{0} \end{Bmatrix}_{\text{ext}} - \begin{Bmatrix} \mathbf{F}_1 \\ \mathbf{F}_2 \\ \mathbf{F}_3 \end{Bmatrix}_{\text{int}} = \begin{Bmatrix} \Delta \mathbf{F}_{1c} \\ \Delta \mathbf{F}_{2c} \\ \Delta \mathbf{F}_{3c} \end{Bmatrix} \quad (5)$$

By rearranging matrix equations we get

$$\begin{aligned} & \left[\mathbf{K}_{21} - \mathbf{K}_{23} \mathbf{K}_{33}^{-1} \mathbf{K}_{31} \right] \{ \Delta \mathbf{u}_1 \} \\ & = \Delta \mathbf{F}_{2c} - \mathbf{K}_{23} \mathbf{K}_{33}^{-1} \Delta \mathbf{F}_{3c} = -\mathbf{F}_{2int} + \mathbf{K}_{23} \mathbf{K}_{33}^{-1} \mathbf{F}_{3int} \end{aligned} \quad (6)$$

We use pseudo-inverse of $\left[\mathbf{K}_{21} - \mathbf{K}_{23} \mathbf{K}_{33}^{-1} \mathbf{K}_{31} \right]$ to solve Eq. (6). However, this does not guarantee zero forces at the measured locations. For further details refer to [12, 13]. Constrained optimization was used to suppress these spurious forces in [12]. Here, we use the Newton's method as an alternate to constrained optimization, as presented below.

$$\mathbf{F}_2(\mathbf{u}_2 + \Delta \mathbf{u}_2) = \mathbf{F}_2(\mathbf{u}_2) + \frac{\partial \mathbf{F}_2}{\partial \mathbf{u}_2} \Delta \mathbf{u}_2 \quad (7)$$

By using the second and third rows of Eq. (5), we obtain

$$\begin{aligned} \Delta \mathbf{F}_{2c} &= \left[\mathbf{K}_{22} - \mathbf{K}_{23} \mathbf{K}_{33}^{-1} \mathbf{K}_{32} \right] \Delta \mathbf{u}_2 \\ &+ \left[\mathbf{K}_{21} - \mathbf{K}_{23} \mathbf{K}_{33}^{-1} \mathbf{K}_{31} \right] \Delta \mathbf{u}_1 \\ &+ \mathbf{K}_{23} \mathbf{K}_{33}^{-1} \Delta \mathbf{F}_{3c} \end{aligned} \quad (8)$$

The gradient of the spurious forces can be expressed as

$$\frac{\partial \mathbf{F}_2}{\partial \mathbf{u}_2} = \left[\mathbf{K}_{22} - \mathbf{K}_{23} \mathbf{K}_{33}^{-1} \mathbf{K}_{32} \right] \quad (9)$$

We use these gradients in the Newton's method to drive the spurious forces to zero. This method converges to a local minimum; hence, we do not need to specify bounds on variable \mathbf{u}_2 . From Eqs. (7) and (9), we can get corrections to measured displacements as follows.

$$\Delta \mathbf{u}_2 = \left[\frac{\partial \mathbf{F}_2}{\partial \mathbf{u}_2} \right]^{-1} \{ \mathbf{F}_2(\mathbf{u}_2) \} \quad (10)$$

4 Prototyping of grippers

The grippers mentioned in Section 2 were fabricated in three different ways: wire-cut Electric Discharge Machining (EDM) (Electronica Model Elektra MAXICUT *e*) and photolithography for spring steel; vacuum casting for polydimethylsiloxane (PDMS).

4.1 Fabrication with spring steel

The advantage of using spring steel for fabrication is that it has uniform and well-characterized material properties and there are standard manufacturing techniques available for spring steel. We used wire-cut EDM to fabricate the grippers of overall dimensions of 11 mm × 11 mm × 0.5 mm as shown in Fig. 6. By using wire-cut EDM, it is possible to manufacture the grippers within the dimensional tolerance of ±20 μm.

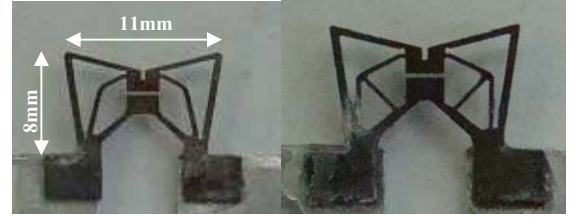
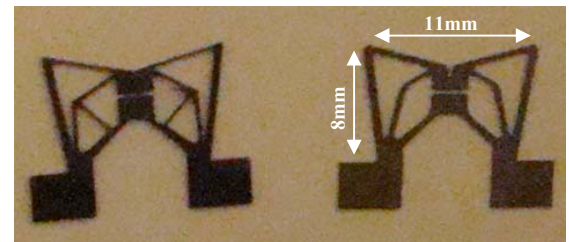


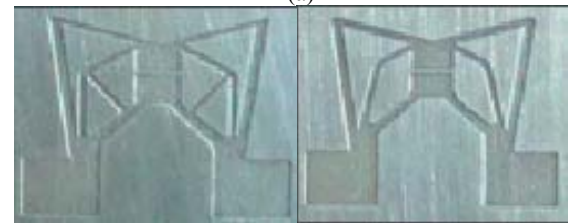
Fig. 6: Spring steel grippers fabricated by EDM.

The photolithography technique was also attempted to fabricate 150 μm thick grippers, which cannot be manufactured by EDM because the pressure of de-ionized water tends to deform the gripper structure during machining. By experimentation, we found that the minimum beam width that can be reliably achieved is 150 μm with our machine.

In photolithography, two conjugate dry-film photomasks were used and the spring steel sheet, coated with photoresist on both the sides, was placed in between the photomasks to get UV exposure on both the sides. To minimize the undercut, both the sides of the gripper were etched simultaneously. Furthermore, the design should account for undercut and should be altered accordingly to get the required dimensions. The grippers made in this way are shown in Fig. 7(a). The savings in time and cost for lithography are substantial as many grippers can be manufactured in one batch. The lithography technique can also be used to make 200 μm deep spring steel moulds for making PDMS grippers. This requires a different set of dry-film photomasks that leave the cavities where the mechanism's material should be. The spring steel moulds etched in this manner are shown in Fig. 7(b). Since the dry-film photomask is still present on one side, the photographs have a bluish-gray tinge.



(a)



(b)

Fig. 7: (a) Spring steel grippers made using lithography and etching and (b) PDMS moulds fabricated by Photolithography.

4.2 Fabrication with PDMS

PDMS is preferred for grippers because of its optical clarity, biocompatibility and low stiffness as compared to spring steel. For manufacturing PDMS grippers, a

spring steel mould for vacuum-casting PDMS was made using wire-cut EDM. The PDMS gel and 10% binder were mixed and poured in the mould after degassing in a vacuum chamber (MK Technology GmbH D-53501 Graf-schaft) for 30 min. PDMS was then cured in an oven (Mettmert W 8540 Schwabach) at 100 °C for 6-7 h. After curing, PDMS gripper was ejected out from the mould. The resultant prototype grippers are shown in Fig. 8. The thickness of the PDMS gripper was set at 2 mm to minimize sagging due to its own weight.

The stiffness of the PDMS gripper shown on the left side of Fig. 8 is 0.024 N/m and that of the one on the right is 80.5 N/m. As compared with the stiffnesses of spring steel grippers (see Figs. 1 and 6), the PDMS grippers have orders of magnitude lower stiffness. By changing the overall size, thickness, and beam width, it is possible to achieve 1 N/m stiffness with PDMS. This is roughly the stiffness of the cell membranes. Thus, it is possible to tailor the stiffness as per the stiffness of the objects grasped or manipulated.



Fig. 8: PDMS grippers fabricated by Vacuum Casting.

5 Micromanipulation

The experiments for micromanipulation were performed using OLYMUS IX71 inverted microscope and 3-axis XYZ stages (SUTTER INSTRUMENT COMPANY MP285) as shown in Figs. 9(a-b). We tested the grippers on spherical-shaped zebrafish egg-cells (~0.7 mm in diameter), ellipsoidal-shaped drosophila (fruit fly) embryos (~0.2 mm wide and ~0.5 mm long), yeast ball (less than 1 mm in diameter), and hibiscus pollen (0.1 mm in diameter). All but the yeast ball are shown in Fig. 10. The drosophila embryo is studied in biology as a model organism because its genome resembles the human genome [14]. In case of zebrafish, which is another popular model organism, the embryo develops organs that are similar to human central nervous system and pancreas [15]. Furthermore, both embryos have good optical clarity.

We were able to grasp, roll, squeeze, position, move, and pick-and-place the aforementioned biological objects along three mutually perpendicular axes in aqueous medium. We achieved a stroke of 0.3 mm using spring steel gripper and hence we have used it for manipulating drosophila embryo and pollen which are of the comparable size. The spring steel gripper is actuated at two points by attaching the ends of the gripper to two different xyz stages using an aluminum strip as shown in Fig. 9c. The dashed arrows show the directions of movement of the two ends. The biological objects were grasped by

first moving the gripper from the top to the plane of the object and later gripper was moved in the plane so as to get the object within the jaws. In the case of the drosophila embryo (see Fig. 10(a)), we were able to draw it into the space between the jaws at one end and let it exit at the other by modulating the motion of the jaws. In the case of pollen, we were able to separate single pollen from the cluster and crush it by repeated action. The contents of the pollen grain that oozed out and stretched between the two jaws can be seen in Fig. 10(b).

We used PDMS gripper for zebrafish egg cells as the stroke of the gripper is around 1 mm. The PDMS gripper used here requires one-point actuation as discussed before. The gripper was fixed on an aluminum plate and attached to one of the XYZ stage. The actuation was done using another XYZ stage as shown in Fig. 9(d). The biological objects were grasped in a similar manner as mentioned above. Figures 9(c-d) show the zebrafish egg cells grasped and then squeezed.

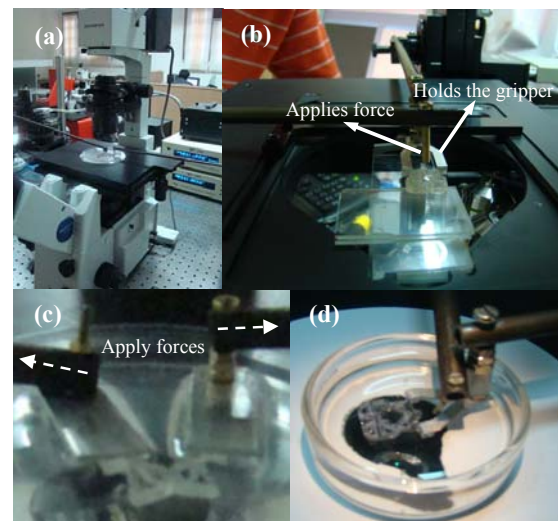


Fig. 9: (a-b) Experimental setup for micromanipulation. (c) two-point actuation for the first gripper, (d) single-point actuation for the second gripper.

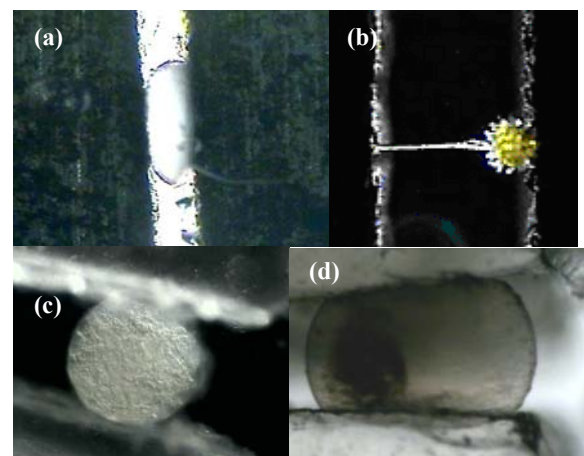


Fig. 10: (a) Drosophila embryo, (b) Hibiscus pollen, (c) Undeformed zebrafish egg cell, (d) Deformed zebrafish egg cell

The PDMS gripper can also be actuated by forceps for grasping micro-sized objects without aqueous medium as shown in Fig. 11(a). The PDMS gripper was attached to the end of forceps using an adhesive and the stroke achieved was 2.5 mm, which enhances the efficiency of grasping small objects even with bare hands. The PDMS gripper used here had parallel jaw motion and it was able to grasp yeast balls as shown in Fig. 11b and we can perform pick-and-place tasks effortlessly.

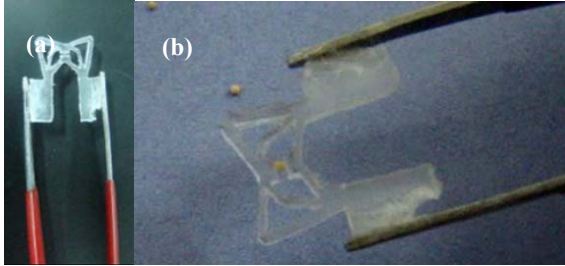


Fig. 11: (a) Enhanced forceps with a PDMS gripper, (b) an yeast ball grasped to do pick-and-place task.

6 Validation, Testing and Results

In this section, we present one computational and two experimental test results to validate the force-sensing technique using miniature compliant grippers described in the earlier sections.

6.1 A criterion for force-sensing

The force-sensing method described in Section 3 does not yield results of the same accuracy for all compliant mechanisms. The reason behind the lack of sufficient accuracy in force-sensing technique was first noticed in case of cantilever beam in [12], where four good examples were presented while the fifth example of cantilever was discussed as the case of inaccurate force-computation. It was argued there that a cantilever is not suited for force-sensing because it has largely mismatched stiffness along its mutually orthogonal directions. When the force-sensing technique was applied to the two grippers presented in the current work, it was found that the gripper shown in Fig. 4 fares much better than the one shown in Fig. 1. Therefore, a pertinent question to ask is: “what decides the suitability of a compliant gripper for force-sensing?” To answer this, we present here a criterion that can serve as a metric.

We want to estimate the ratio between maximum and minimum principal stiffnesses which measures the highest mismatch of stiffness. The large mismatch in stiffnesses along the orthogonal directions in a cantilever beam implies that the principal stiffness ratio is high. The advantage with the ratio criterion is that it can be generalized for the case where we have to estimate forces at multiple locations. The principal stiffness ratio can be obtained from the sensitivity matrix of estimated forces with respect to measured displacements. In order to get the correct sensitivity matrix, spurious forces have to be suppressed. For this, we need to solve the inverse problem by perturbing each and every measured degree-

of freedom to get the corresponding sensitivity matrix. To avoid this extensive computation, forces were applied in a sequence at desired locations (in Figs. 12(a-e), we labeled these locations as **B**) and a set of displacement vectors were computed at measured locations (in Figs. 12(a-e), we labeled these locations as **M**). Hence, in this process, additional computation of spurious forces is avoided. Using sets of computed displacements, a new rectangular matrix is obtained. We then convert it to a square matrix to calculate the condition number. The square matrix is obtained by multiplying the transpose of rectangular matrix with itself. We now define the metric as the condition number of this square matrix.

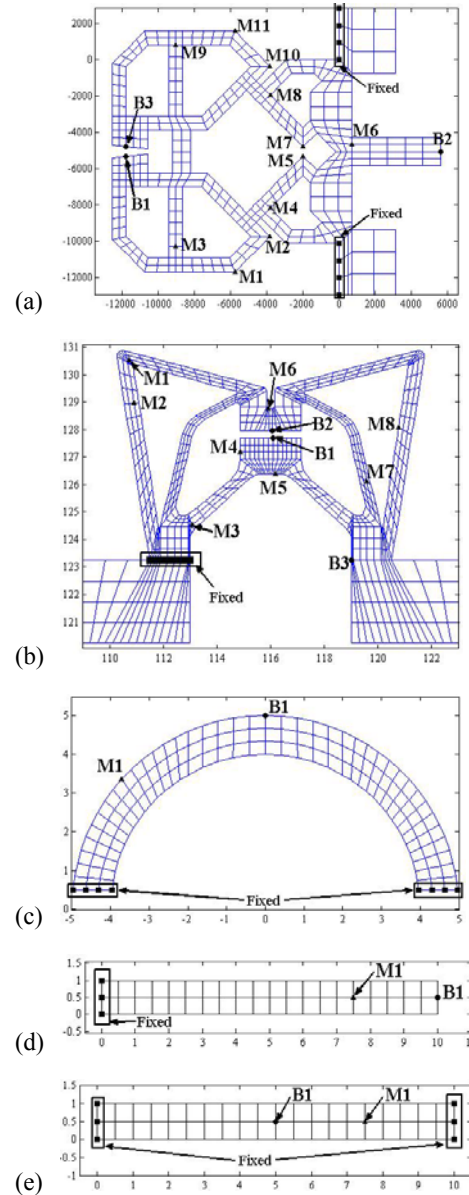


Fig. 12: Five examples of compliant mechanisms or flexible structures chosen for force estimation. The values of the metric were computed to be: (a) 4.987e2, (b) 1.563e5, (c) 6.744e2, (d) 9.187e4, and (e) 6.114e2. Since the metric should be less than 1000, only (a), (c), and (e) work well.

If the metric is lower than 1000, we say that the compliant mechanism/structure is suitable for force-sensing. This is because low condition number gives more stability to the solution.

We show six compliant mechanisms or flexible structures in Figs. 12(a-e) along with their metrics. The first two are the compliant grippers considered in this work. The third structure is arch fixed at both ends. The fourth one is a cantilever beam fixed at the left end with one measurements point. The fifth structure is a fixed-fixed beam with a single measurements point.

The first, third, and fifth examples shown in Figs. 12(a), 12(c), and 12(e), work well for good force-estimation whereas the second (Fig. 12(b)) and fourth (Fig. 12(d)) do not. This inference is clear from the metrics corresponding to these mechanisms as shown in the caption of Fig. 12.

6.2 Testing of the Newton's method using synthetic data

For numerically validating the force-computation technique, we considered the gripper whose geometry is shown in Fig. 12(a). The measurement locations are indicated with label M and nodes where the forces were applied are labeled as B. The thickness of the gripper is 2 mm, Young's modulus of the material is 1.5 MPa and Poisson's ratio is 0.48. Computed and applied forces are shown in the Fig. 13. We introduced 15% error in the displacements and observed the maximum error in computed forces to be about 15%.

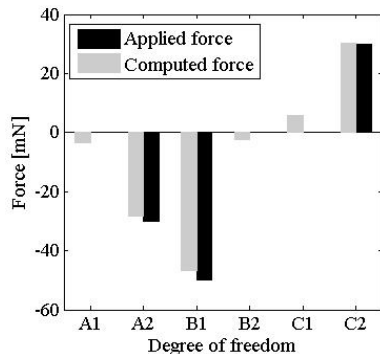


Fig. 13: Comparison of computed and applied forces with Newton's method

6.3 Force estimation on a yeast ball

In this case, we performed an experiment on a yeast ball to compute the contact forces of grasping it. The PDMS gripper geometry is shown in Fig. 12. The undeformed and deformed configurations of the gripper were captured using a CCD camera (Sentech STC-625AS) as shown in Fig. 14. We extracted the displacements with the help of Image-pro software. Computed forces are presented in Fig. 15. The forces acting on the yeast were found to be about 30 mN.

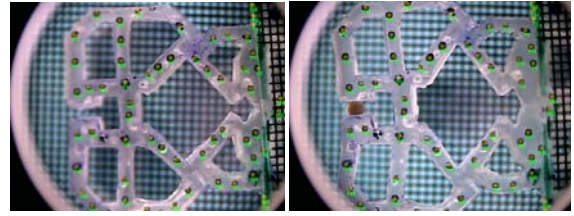


Fig. 14: Undeformed and deformed configurations of PDMS gripper

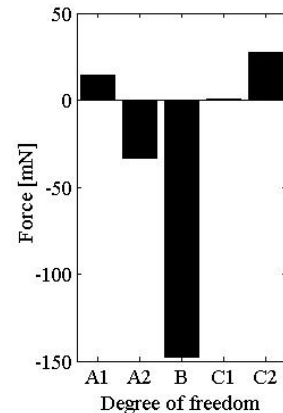


Fig. 15: Computed forces on yeast

6.4 Macro scale experiment

In the previous subsection, we computed forces at small scale. It is a difficult task to validate these forces independently unless we have another method of force-sensing. Even then, we cannot be sure of the errors in the other sensor. Hence, we performed one experiment on a macro-scale gripper fabricated using polypropylene with help of a CNC machine (FANUC Seires Oi-MC VMC-850). This gripper is shown in Fig. 16.

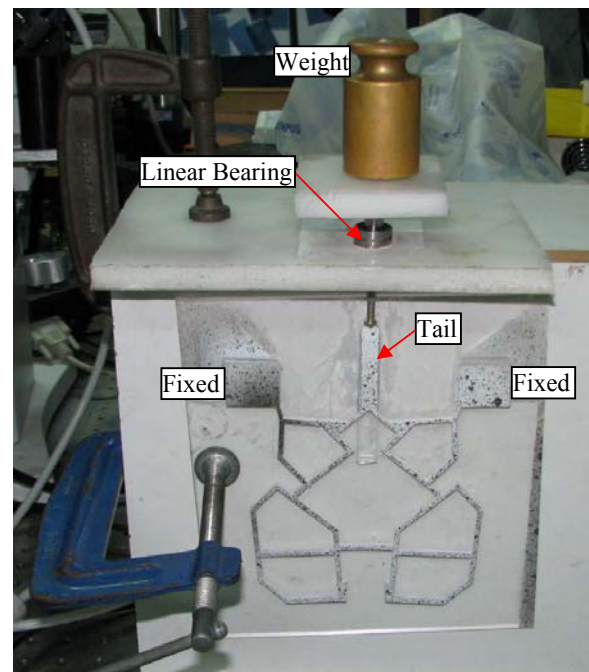


Fig. 16: Experimental setup of macro-gripper

The size of gripper is 172 mm × 149 mm, which allows us to measure forces independently at both the jaws. A linear bearing was used to apply the load to the tail of the gripper. To measure the displacements at various locations, we sprayed dark paint on the gripper. We then attached a camera (Canon Powershot S5) to capture images of the gripper before and after deformation. The displacement was measured using Image-pro software by comparing location of absolute coordinates in the two images.

We first evaluated the Young's modulus of the gripper's material by actuating the gripper without holding any object. The actuation force was applied using dead weights at the end of the tail of the mechanism as shown in Fig. 16. Displacements extracted at the tail by looking at the deformed configuration shown in Fig. 17(a) along with the undeformed configuration. The measured force was applied in the COMSOL model and the Young's modulus was varied until the simulated displacements were in agreement with the experimental values. Experimental and simulated deformations are shown in Fig. 17. This Young's modulus, computed to be 1.2 GPa, was used in the computation of force on holding an object.

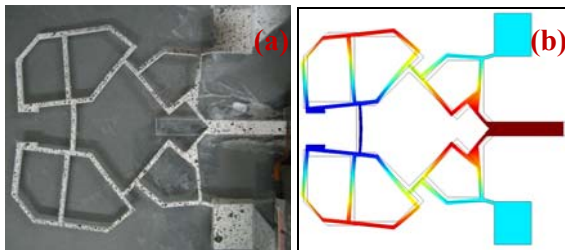


Fig. 17: Deformed configuration of the gripper without holding an object (a) Experimental image (b) Simulated deformation using COMSOL software. This was to estimate the Young's modulus of the material.

The experiment for calculating the gripping forces was done by transferring to a spring via levers as shown in Fig. 18. This arrangement ensures no buckling of the spring because of the tensile load. The spring force was calculated by measuring the deflection using Image-Pro software. The gripping forces were computed using our force-sensing algorithm based on the Newton's method described in Section 3 and forces are shown in Fig. 19. The comparison of experimental and computed results is shown in Table 1. It can be seen that the maximum error in the computed forces is 7.5%.

6.5 Testing of Newton's method for random errors

We also tested the solution of the Cauchy inverse problem solved using the Newton's method on a 3 mm thick gripper of the kind as shown in Fig. 12(a). Young's modulus and Poisson's ratio of the material were taken as 1.5 MPa and 0.48. We applied 0.1125 N horizontal force (actuation force at the end of tail) and 0.0187 N vertical force at jaws to obtain synthetic data. We got 324 μm and 111.2 μm as maximum and minimum displacements at specified locations (these locations indi-

cated with label 'M' in the Fig. 12(a)). The error introduced in displacements was less than or equal to ±5 μm using a random number generator. Therefore, the maximum % error in displacements is less than 5%. In order to show that the estimated force is less than 5%, we performed 2000 runs of the programme with different random errors in displacements within 5%. The error distribution plot is shown in Fig. 20.

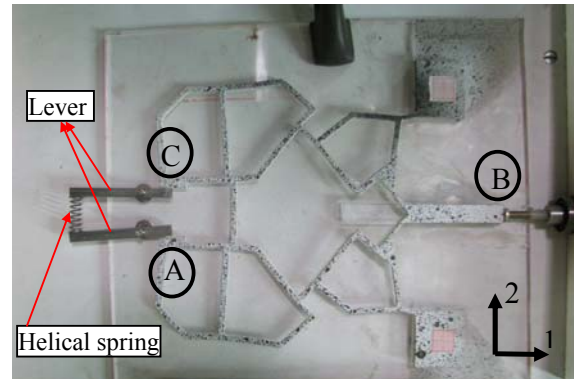


Fig. 18: Experimental setup or measuring gripping forces

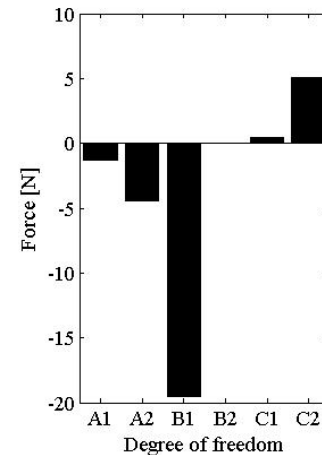


Fig. 19: Computed forces on macro-gripper at the locations A, B and C

Table-1: Comparison of experimental and computational forces in the macro-scale experiment

Location	Computed force (N)			Measured force (N)
	Horizontal	Vertical	Total	
A	-1.26	-4.27	4.57	4.94
B	-19.5	0.04	19.5	20.95
C	0.48	5.07	5.09	4.94

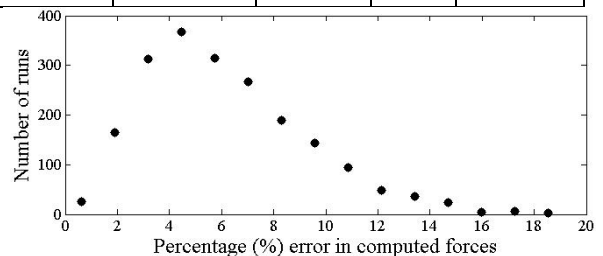


Fig. 20: Error distribution with number of runs

It can be seen that the peak of the distribution occurs at about 5% while there are a few runs that incurred larger than 5% error and very few incur more than 10% error. Hence, we can say that the method works reasonably well in the sense that the error in the estimated force is rarely more than twice the error in the measured displacements.

7 Closure

In this paper, we presented miniature-grippers using which we could grasp and manipulate biological objects that are smaller than 1 mm in diameter and are immersed in aqueous medium. One type of gripper and its two variants were designed intuitively while the second type was designed using topology optimization that incorporated manufacturing considerations. The grippers were made using wire-cut electro-discharge machining (EDM), chemical etching, and vacuum-casting using spring steel and polydimethylsiloxane materials. The grippers can also act as force sensors by virtue of our vision-based force-sensing technique. Here, we presented an alternative technique based on the Newton's method for solving an inverse problem, called the Cauchy problem in elasticity. This is an improvement over our earlier solution method of the same equation. We described the experimental setup and how we grasped and manipulated zebrafish egg cells, drosophila embryos, yeast balls, and grains of pollen. We estimated the forces applied on a yeast ball as 30 mN. For validating our technique, we performed a numerical experiment and also a macro-scale experiment where we used a spring-lever setup to estimate forces independently. We showed that the forces computed were of the same order of magnitude, which may be acceptable in experiments involving small biological objects manipulated in their native aqueous medium.

Acknowledgments

The authors would like to thank Sudarshan Hedge for helpful discussions; Sridhar (CPDM), Ramu, Vinod and Ravi for their help in fabrication of grippers. This work is supported in part by the Swarnajayanthi fellowship of the Department of Science and Technology (DST), Government of India, to the fourth author as well as the Math Biology grant from DST (No. Sr/S4/MS; 419/07).

References

[1] A. Ashkin, "Acceleration and Trapping of Particles by Radiation Pressure", *Physical Review Letters*, Vol. 24, 1970, pp. 156-159.
[2] T.N. Bruican, M.J. Smyth, H.A. Crissman, G.C. Salzman, C.C. Stewart, J.C. Martin, "Automated Single-Cell Manipulation and Sorting by Light Trapping", *Applied Optics*, Vol.26, 1987, pp. 5311-5316.

[3] M. Nishioka, S. Katsura, K. Hirano, A. Mizuno, "Evaluation of Cell Characteristics by Step-Wise Orientational Rotation Using Optoelectrostatic Micromanipulation", *IEEE Transactions on Industry Applications*, Vol. 33, 1997, pp. 1381-1388.
[4] M. Dafflon, B. Lorent, R. Clavel, "A micromanipulation setup for comparative tests of microgrippers", *International Symposium on Robotics, Munich, 2006*.
[5] S. Yu, B.J. Nelson, "Autonomous Injection of Biological Cells Using Visual Servoing", *Experimental Robotics VII, LNCIS 271*, 2001, pp. 169-178.
[6] S.K. Nah, Z.W. Zhong, "A microgripper using piezoelectric actuation for micro-object manipulation", *Sensors and Actuators*, Vol.133, 2007, pp. 218-224.
[7] M.N.M. Zubir, B. Shirinzadeh, "Development of a high precision flexure-based microgripper", *Precision Engineering*, 2008.
[8] D.K. Sahu, G.K. Ananthasuresh, "Optimal Design of a Meso-scale Gripper and its Prototyping with Spring Steel and PDMS", *International Conference on Smart Materials Structures and Systems, Bangalore, 2008*.
[9] X. Wang, G.K. Ananthasuresh, J.P. Ostrowski, "Vision-based sensing of forces in elastic objects", *Sensors and Actuators A Physical*, Vol.94, 2001, pp. 142-156.
[10] M.A. Greminger, B.J. Nelson, "Vision-based forces measurement", *IEEE Trans. Pattern Analysis and Machine Intelligence*, Vol.26, 2004, pp. 290-298.
[11] K. Kamiyama, K. Vlack, T. Mizota, H. Kajimoto, N. Kawakami, S. Tachi, "Vision-based sensor for real time measuring of surface traction", *IEEE Computer Graphics and Applications*, Vol.25, 2005, pp. 68-75.
[12] A.N. Reddy, G.K. Ananthasuresh, "On computing the forces from the noisy displacement data of an elastic body", *International Journal for Numerical Methods in Engineering*, Vol.76, 2008, pp. 1645-1677.
[13] M.A. Crisfield, *Non-Linear Finite Element Analysis of Solids and Structures*, John-Wiley and Sons, New York, 1997.
[14] R.W. Bernstein, X. Zhang, S. Zappe, M. Fish, M. Scott, O. Solgaard, "Characterization of fluidic microassembly for immobilization and positioning of Drosophila embryos in 2-D arrays", *Sensors and Actuators*, Vol.114, 2004, pp. 191-196.
[15] D.H. Kim, S. Yun, B. Kim, "Mechanical Force Response of Single Living Cells Using a Microrobotic System", *IEEE International Conference on Robotics and Automation, Hilton New Orleans Riverside, New Orleans, LA, USA*, Vol.5, 2004, pp. 5013-5018.